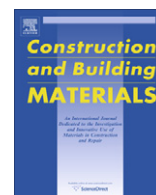




Contents lists available at ScienceDirect

Construction and Building Materials

journal homepage: www.elsevier.com/locate/conbuildmat

NDT approach for characterization of subsurface cracks in concrete

D.G. Aggelis*, E.Z. Kordatos, M. Strantza, D.V. Soulioti, T.E. Matikas

Department of Materials Science and Engineering, University of Ioannina, 45110 Ioannina, Greece

ARTICLE INFO

Article history:

Received 24 September 2010

Received in revised form 23 December 2010

Accepted 24 December 2010

Keywords:

Nondestructive testing
Thermography
Cooling down
Longitudinal wave
Rayleigh wave
Ultrasound
Simulation

ABSTRACT

A combination of nondestructive testing techniques is applied in this paper for the detection and characterization of subsurface damage in concrete. Thermography is initially used to locate the defects, in the form of vertical cracks beneath the surface, due to the variation of the temperature field as monitored by an infrared camera. Additionally, cooling down curves enhance the characterization by the different rate of heat exchange between cracked and sound areas. Consequently ultrasound propagation is used to estimate the depth, by the firm correlation between wave transmission and damage characteristics. The complementary use of the two techniques is discussed as a potential robust methodology for evaluation of difficult damage in concrete before it is visible.

© 2010 Elsevier Ltd. All rights reserved.

1. Introduction

Subsurface cracking in concrete may be the result of reinforcement corrosion, or delaminations between successive layers. This damage is not visible until it breaks the surface and allows rapid deterioration of the structure due to penetration of water and other environmental agents. The detection of this kind of damage enables repair either by replacement of the surface layer or by cement injection [1]. Since early assessment is desirable, passive means of monitoring the onset of corrosion and early corrosion-induced cracking have been examined in laboratory [2]. Considering the large surface area of typical concrete structures the assessment should be quick, global, and accurate. For this purpose suitable nondestructive testing (NDT) techniques should be utilized. Thermography is established as an effective technique for investigation of civil structures. Defects or inhomogeneities which lie below the surface affect the heat transfer rate when thermal energy is propagating into or out of the structure. This can be monitored by an infrared camera and the positions of the flaws are determined by the temperature variations on the surface. It is a common method successfully applied for inspection of delaminations, moisture or quality of insulations in concrete or masonry structures [3–6]. Therefore, it fulfils the first prerequisite of testing because it can monitor a large surface area by just one thermographic image. When the defect is identified, another technique can be used for more accurate characterization of its depth. One of the most

promising techniques for this task is ultrasound, since several wave parameters are influenced by the presence of cracks [7,8]. These could be mainly velocity or amplitude which decrease when the wave propagates through damaged volumes, as well as other more advanced frequency or dispersion features [9,10].

In this study, steel fiber-reinforced concrete (SFRC) specimens with subsurface cracks were scanned by an infrared camera after being heated in an oven in order to identify the position of the subsurface crack. Consequently the specimens were examined by one sided ultrasonic measurements and crucial parameters of wave propagation were correlated with the depth to the crack. Preliminary results [11] showed that infrared images of specimens at high temperatures of 90 °C, could indicate the position of damage, while elastic wave parameters like amplitude and velocity were certainly influenced by underlying cracking. Based on these encouraging results many details were improved in the next step. The thermography analysis was conducted at approximately 60 °C, which is quite close to the temperature of concrete under direct sunlight, making thus the study more realistic. Additionally, the temperature field was monitored for a period of two hours in order to enhance the characterization by information on the cooling down curve of the material. Another important feature is that the cracks were developed under different mid-span deflection of the specimens, which enabled the creation of different lengths of cracks. Consequently this study, enables not only crack detection, which was conducted in [11], but also estimation of depth-to-crack. Concerning elastic wave simulations, a more realistic crack shape was used to account for smaller side cracks, which inevitably escort the main crack when SFRC is damaged. The fusion of information gathered by

* Corresponding author. Tel.: +30 26510 08006; fax: +30 26510 08054.

E-mail address: daggelis@cc.uoi.gr (D.G. Aggelis).

infrared thermography and elastic waves provides effective means for inspection of concrete [12].

2. Materials

The specimens were made of steel fiber-reinforced concrete (SFRC). Their size was $100 \times 100 \times 400$ mm. The water to cement ratio by mass was 0.5 and the aggregate to cement ratio 3.6. The maximum aggregate size was 10 mm. The fiber content was 0.5%, by volume. The reason for fiber inclusion was to control the mid-span deflection and therefore the penetration of the crack to the top surface, since plain concrete would fail catastrophically in two parts after the main crack formation. The specimens were tested in 4-point bending according to ASTM C1609/C 1609 M-05, see Fig. 1a, resulting in approximately vertical cracks which propagated from the bottom tensile surface to the top. More details on the materials and the flexural test are supplied in [13]. Fig. 1b and c shows side views of two specimens with different deflections. The main crack is accompanied by smaller cracks but there is no visible sign of them from the compression side. Totally seven specimens were produced from the same mix and were loaded up to different levels of mid-span deflection, see Table 1, in order to produce cracks with different lengths. In the same table, the distance between the tip of the crack and the top surface is included, as measured from the side.

3. Thermography

The experimental setup includes an infrared camera and an oven. The type of the camera was Flir T360 with a spectral range of $7.5\text{--}13\ \mu\text{m}$ and a sensitivity of $0.06\ ^\circ\text{C}$ at $30\ ^\circ\text{C}$. The energy source employed for the heating of the specimens was an oven with temperature range $20\text{--}200\ ^\circ\text{C}$. The infrared camera was placed at 1.6 m distance from the specimens, see Fig. 2. The specimens were placed horizontally on a metal stand without any additional mounting. The top of the stand is coated with a non thermal material to avoid heat dissipation from concrete. The thermal emissivity of concrete is 0.92 [14] and there was no need to paint the surface. Experiments were conducted in laboratory under constant conditions of air temperature of $23\ ^\circ\text{C}$ and relative humidity 70%. Thermographs were recorded after the specimens were heated in the oven at $90\ ^\circ\text{C}$ for 3 h. The oven was used as an easy and suitable way to produce uniform temperature in the whole volume of the specimen.

3.1. Thermographic images

Figs. 3a–9a show the thermograms of all specimens. The vertical dash lines included in some of the figures will be discussed in the next section. For most of the specimens there is a distinct variation in the temperature field at the area on top of the crack. This local decrease in temperature is reasonable according to the thermal diffusivity of the materials. Concrete exhibits much lower thermal diffusivity than air. Therefore, cooling is much slower in the bulk of the material than near the crack that contains air [4].

Table 1
Specimens and crack dimensions.

Specimen	Mid-span deflection (mm)	Distance between crack tip and top surface* (mm)
A	3	3
B	2.5	4
C	2.2	6
D	2	10
E	1.5	11
F	1	12
G	0.5	29

* As measured from the side.

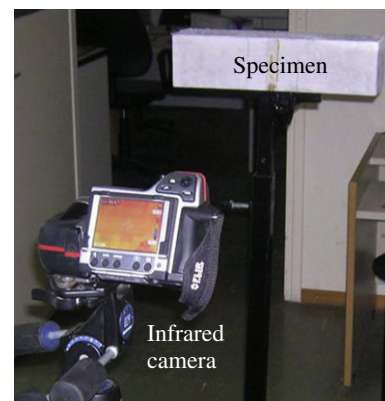


Fig. 2. Photograph of the thermographic experiment.

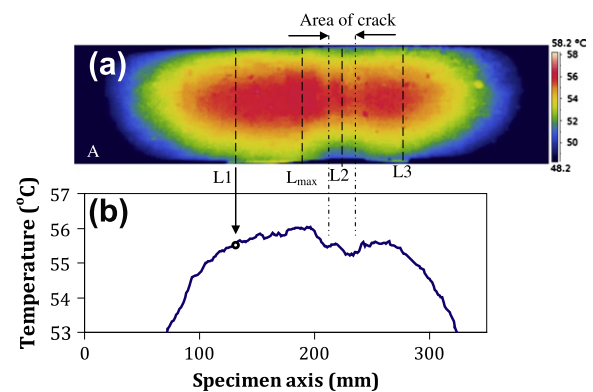


Fig. 3. (a) Thermograph of the specimen with mid-span deflection 3 mm and (b) average temperature along the specimen's axis.

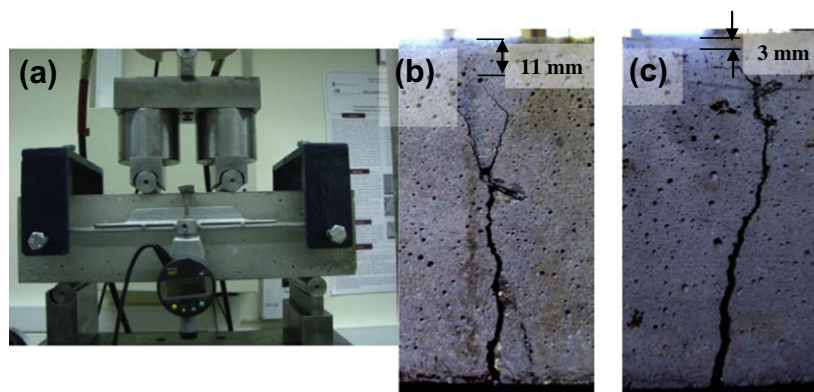


Fig. 1. (a) Experimental setup for creating cracks in concrete through 4-point bending. Two typical specimens after bending with mid-span deflection 1.5 mm (b) and 3 mm (c).

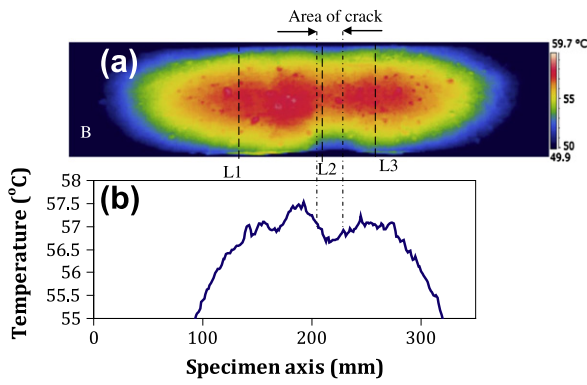


Fig. 4. (a) Thermograph of the specimen with mid-span deflection 2.5 mm and (b) average temperature along the specimen's axis.

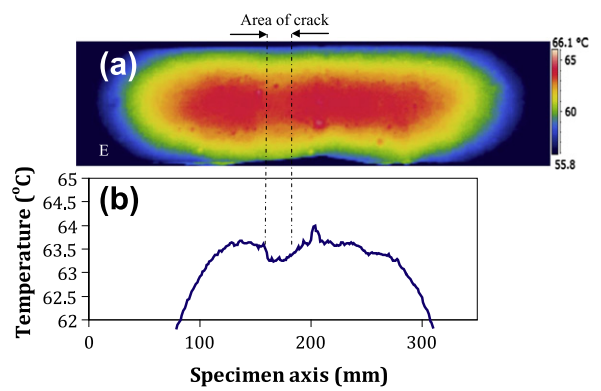


Fig. 7. (a) Thermograph of the specimen with mid-span deflection 1.5 mm and (b) average temperature along the specimen's axis.

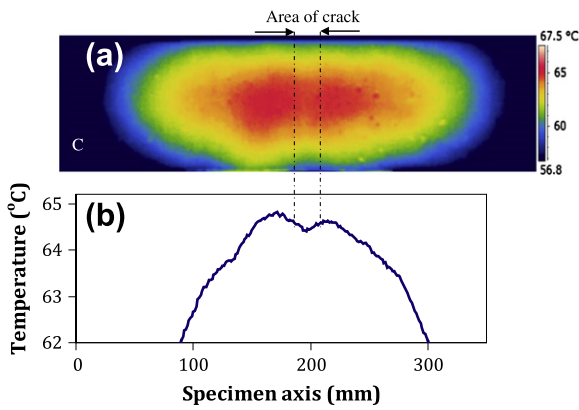


Fig. 5. (a) Thermograph of the specimen with mid-span deflection 2.2 mm and (b) average temperature along the specimen's axis.

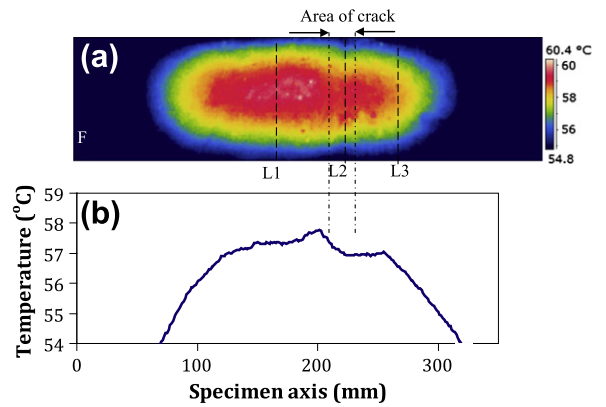


Fig. 8. (a) Thermograph of the specimen with mid-span deflection 1 mm and (b) average temperature along the specimen's axis.

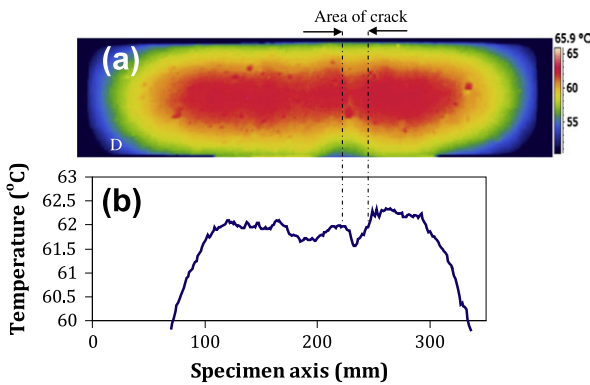


Fig. 6. (a) Thermograph of the specimen with mid-span deflection 2 mm and (b) average temperature along the specimen's axis.

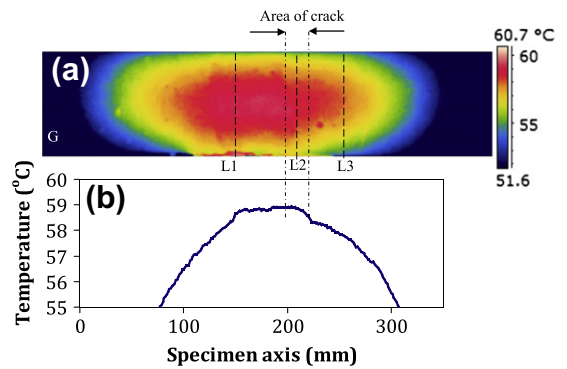


Fig. 9. (a) Thermograph of the specimen with mid-span deflection 0.5 mm and (b) average temperature along the specimen's axis.

This is more clear for the specimens with deeper cracks (Figs. 3a–6a, specimens A–D), since the cracks extend very close to the monitored surface. This temperature variation is manifested by a narrowing of the zone with the highest temperature (red¹ in the color bar) at the area of the crack. Despite, the thin crack tip, which may have a very small projection on the surface compared with other type of damage like delaminations, it still results in a slight difference on the temperature surface of the order of 1 °C, which can be

¹ For interpretation of color in Figs. 3–10, the reader is referred to the web version of this article.

readily captured by the infrared camera. As the cracks become smaller for the next specimens (Figs. 7a–9a), this narrowing of the warm zone becomes less obvious, and especially for the specimens with deflection of 1 mm and 0.5 mm (specimens F and G respectively), for which the crack is approximately 12 mm and 28 mm away from the monitoring surface, there is no certain visible trace of the underlying damage.

It is mentioned that although the specimens were heated up to 90 °C, the thermographs are taken for temperatures of around 60 °C. This is for practical reasons since in actual conditions, even during a sunny day, the temperature of concrete surface will not

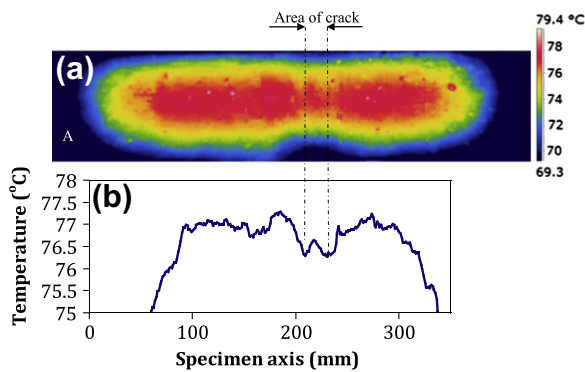


Fig. 10. (a) Thermograph of the specimen with mid-span deflection 3 mm (same with Fig. 3a) at high temperature range and (b) average temperature along the specimen's axis.

rise above 60 °C. However, it is mentioned that thermograms at 80 °C are much clearer as shown in Fig. 10 where the temperature field of specimen A is depicted. The location of the defect of specimen A is much clearer than shown in Fig. 3a. Although such a temperature is not possibly the result of direct sunlight, it is useful for potential cases of application with lamp heaters in order to enhance the detection of deeper and smaller defects [15,16].

3.2. Average temperature

As introduced in [11] a simple way to enhance the detection capability is by considering the average temperature of vertical lines, see Fig. 3b. This procedure involves averaging of the temperature of the whole number of pixels on successive vertical lines. Specifically, the thermographs in this study were represented by 320x48 pixels. The average temperature of each column (e.g. Line 1 in Fig. 3a) which includes 48 values is depicted in Figs. 3b–9b for all specimens. At the point of the actual crack in most cases (except F and G) a local minimum of the curve is exhibited, excluding of course the areas near the left and right edges of the specimens which are cooling down more quickly. The above mentioned procedure enables more reliable characterization, because some random, small defects on the surface (e.g. air voids) although may influence the temperature of a few pixels in the near vicinity, they are not enough to influence the average of 48 values of temperature from the pixels on a straight vertical line. Therefore, even slight changes of temperature owing to the subsurface defect can be evaluated. It is mentioned that for higher temperatures (e.g. 75 °C) the average line shows much clearer indication due to the strong local minimum, see Fig. 10b, in comparison to Fig. 3b which was taken at the temperature of 55 °C on the same specimen.

3.3. Cooling down curves

The above methodology is proved successful in the detection of the “troublesome” areas. This analysis is based on a transient image of the temperature field. However, monitoring the cooling down curve can also be studied in order to confirm or even improve the results. It has been used to supply information on the depth of artificial voids [6,12]. As mentioned earlier, the subsurface defect influences the heat rate from the specimen to the environment. This has an effect not only on a specific “snapshot” of the temperature field but also on the cooling rate. Fig. 11a shows the average temperature for three vertical lines of specimen A, (L1, L2, L3, in Fig. 3a) as a function of time. Line 2 is located exactly on the projection of the crack, while L1 and L2 to either sides of the crack on sound material. All of them can very well be fitted

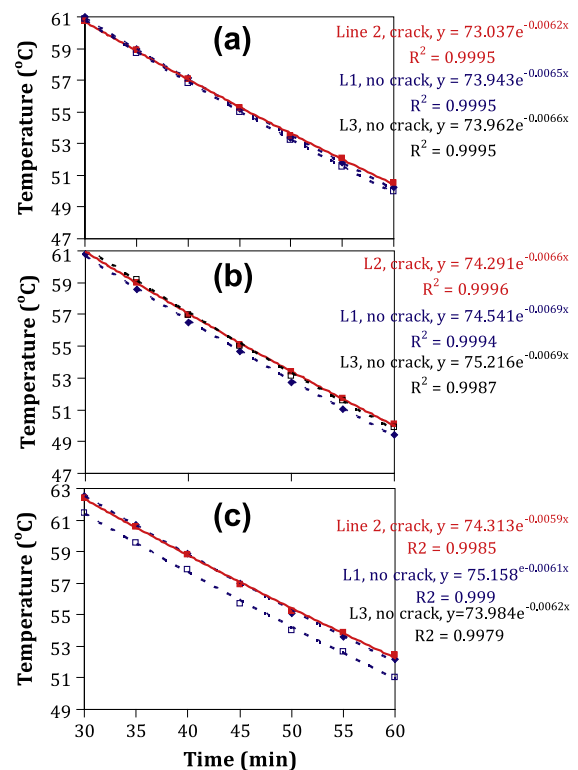


Fig. 11. Cooling down curves for specific vertical lines of specimens: (a) A, (b) B and (c) F.

by exponential decay curves, as seen by the correlation coefficient which is almost unity. However, the exponential superscript is lower for the case of line L2 located on the crack (0.0062 compared to 0.0065 for uncracked). This is a repeatable trend especially for the initial part of the cooling stage when the heat exchange is strong. Fig. 11b and c shows the cooling down curves for vertical lines L1, L2 and L3 for specimens B and F. For all cases the exponential factor of the cooling off curve corresponding to the crack (Line 2) is lower. Even for the specimen with the crack 12 mm below the surface (Fig. 11c), the exponent of the cooling down curve for L2 is certainly lower than the neighboring “healthy” areas. This difference may be of the order of 2%, and does not crucially affect the shape of the curve; its repeatability however, makes it another descriptor to take seriously into account for subsurface damage detection.

Therefore, it is suggested that calculation of the exponent of the cooling off curve for a short period of time (for this case 30 min) along the specimen's axis can indicate the position of the crack by a global minimum of the exponent over the monitored surface, similarly to the minimum of the average temperature.

It should be mentioned that the cooling down curves start again at the point when the temperature has fallen from 80 °C to around 60 °C for practical reasons of applicability in situ (in this case 30 min after the specimens were reduced from the oven). However, the study of the curves from the beginning of the cooling off stage (0–30 min) results in similarly or more clear differences in the exponent.

It is interesting to examine the temperature difference between a defective area and a sound one. In previous studies this difference, as a function of time, was found to obtain a maximum according to the depth of the defect [6]. Fig. 12 shows the difference between the temperature above the crack (line L2) and the maximum-temperature line, considered indicative of sound material (e.g. L_{max} in Fig. 3a), for different specimens as a function of

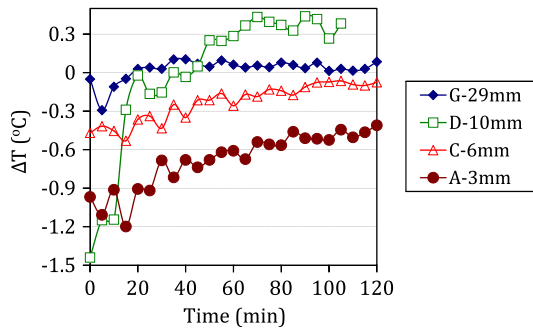


Fig. 12. Temperature difference between the crack location and the maximum temperature of four specimens (the legend includes the distance of the crack from the surface for each specimen).

time. For the curve of specimen G (smallest crack), the discrepancy is not very strong; initially the temperature on the defect is slightly lower and after 20 min, there is no considerable difference between cracked and sound portion of the material (less than 0.1 °C). As the crack reaches the surface, the discrepancy becomes more significant, as seen in Fig. 12 for specimens C and A. For A with the largest crack (only 3 mm from the monitored surface), the initial difference is more than 1 °C, while the cooling down time of 2 h is not enough to equalize the temperature between the defective and sound areas of the specimen. This behavior is reasonable due to the size of the defect that imposes changes in the heat rate which are still evident even after long period of time. However, the result is not consistent since other specimens, with nominally smaller cracks do not follow this trend, as seen by the curve of specimen D (see again Fig. 12). In this case the crack is approximately 10 mm away from the surface, but the difference is almost 1.5 °C at the start of the monitoring period, while after about 40 min the defective area obtains temperature approximately 0.4 °C higher than the sound area. The lack of repeatability for all specimens is indicative of the inhomogeneous nature of damage in concrete. In several approaches where artificial defects are placed inside concrete in the form of thin plates, the results are much clearer, more likely due to the large projection of the defects on the monitored surface [6,12,16]. However, when vertical cracks are considered—and the conditions become more realistic—the projected area of the defect on the monitored surface cannot be accurately controlled. Therefore, although a crack may be measured at a certain distance from the surface, the internal geometry of the crack may be different leading to heat exchange rates different than expected. This also shows that information of thermography (transient temperature field, averaging of temperatures over a mesh, cooling down rate) may well indicate the damage even in the form of thin crack tips a few cm from the surface, but another more detailed assessment should follow for more precise determination of the depth. The use of ultrasound discussed below aims at more accurate estimation of the depth of the subsurface crack at the location pointed out by thermography.

4. Ultrasound

Elastic wave parameters such as velocity and attenuation are quite sensitive to the existence of damage, either in the form of distributed micro-cracks [8,9], as well as large macroscopic voids [17,18]. Specifically, surface waves have been used in many cases for detection of surface or near surface damage as they occupy most of the energy after any excitation and propagate only on the surface, penetrating approximately to a depth equal to their wavelength. Therefore, they are considered suitable for characterizing damage in concrete [18,19].

4.1. Experimental setup

The experimental setup for the elastic wave measurements is depicted in Fig. 13a. Two sensors were placed on the intact side of the specimen at a distance of 70 mm. The excitation was conducted by pencil lead break which introduces a frequency band up to approximately 300 kHz. The sensors were acoustic emission transducers (Physical Acoustics, PAC Pico), with broad band response from 50 kHz to 800 kHz and diameter of 5 mm. The sampling frequency of the acquisition board was set to 5 MHz.

Wave velocity was measured by the time delay between the waveforms collected at the different sensors. Typical waveforms recorded on sound material are depicted in Fig. 13b. For pulse velocity determination the first disturbances (wave onsets in Fig. 13b) were used. The onset corresponds to the longitudinal wave which is the fastest type. Rayleigh wave velocity was measured by the strong characteristic peaks (see arrows in Fig. 13b) of the Rayleigh burst which stand higher than the initial longitudinal arrivals due to their higher energy [19]. Fig. 13c shows typical waveforms for cracked concrete. The waveform of the 1st receiver is not much influenced since this sensor is located before the crack. The waveform of the 2nd receiver though, is very weak, since most

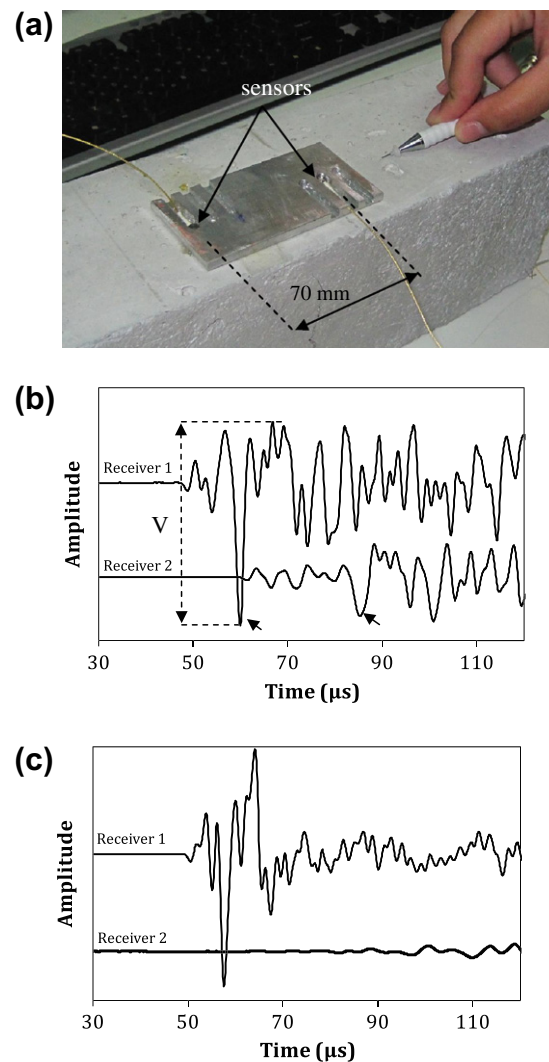


Fig. 13. (a) Experimental setup, Typical waveforms, (b) for sound concrete and (c) for cracked concrete (specimen A with distance from the surface to crack tip 3 mm). The arrows in (b) indicate the Rayleigh peaks.

of the energy was reflected on the crack while it is not possible to distinguish the Rayleigh peak. The measurements were repeated ten times by slightly translating and rotating the receivers array around the crack and the results were averaged. Results will be presented along with simulation ones.

4.2. Elastic wave simulation

In the present case, in order to create the subsurface cracks, the specimens were subjected to 4-point bending with monitoring of their mid-span deflection. This was applied in order to lead to actual cracks and make the study more realistic. However, the deflection of the specimen does not directly correspond to an exact depth of the crack, mainly due to the heterogeneity and randomness of concrete and its damage mechanisms. Using simulations, the depth-to-crack can be exactly resembled in order to lead to specific curves, between wave parameters and depth-to-crack. In this case a main crack with small diagonal cracks was simulated, for as many as 14 different depths.

Commercial software was used which operates by solving the two-dimensional elastic wave equations based on a method of finite differences [20,21]. The material was considered elastic neglecting viscosity. The Lamé constants were $\lambda = 12$ GPa and $\mu = 16.5$ GPa, with density of 2400 kg/m^3 , resulting in a longitudinal wave velocity of 4300 m/s similar to the healthy SFR concrete. The corresponding elastic modulus is 40 GPa and Poisson's ratio 0.2 . For the crack material modeling, properties of air were applied, leading to wave velocity of 300 m/s .

The geometric model was of rectangular shape with 100 mm thickness to resemble the experimental specimen, see Fig. 14. The mesh size of the calculation was set to 0.2 mm much smaller than the longitudinal wavelength of 43 mm , and the Rayleigh of 24 mm ensuring accurate solution. In order to reduce the calculation time, the specimen's length was reduced to the center 200 mm and infinite boundary conditions were applied to the opposite sides, cancelling the reflections from the edges [11]. The two simulated receivers were 5 mm long to resemble the actual transducers and were placed on the top side of the specimen with a separation of 70 mm . The receivers computed the average lateral displacement on their defined length. The simulated cases concerned the crack-free geometry, as well as geometries with subsurface cracking at several different depths, namely 80 mm , 60 mm , 40 mm , 30 mm , 25 mm , 20 mm , 16 mm , 12 mm , 10 mm , 8 mm , 6 mm , 4 mm , 2 mm and 1 mm . The crack had a thickness of 1 mm , while small inclined side cracks were also considered to better resemble the geometry of the actual cracks in SFRC, see Fig. 14. The excitation was simulated by one cycle of 20 kHz , 100 kHz and 200 kHz , while in this paper, results from 20 kHz and 200 kHz are

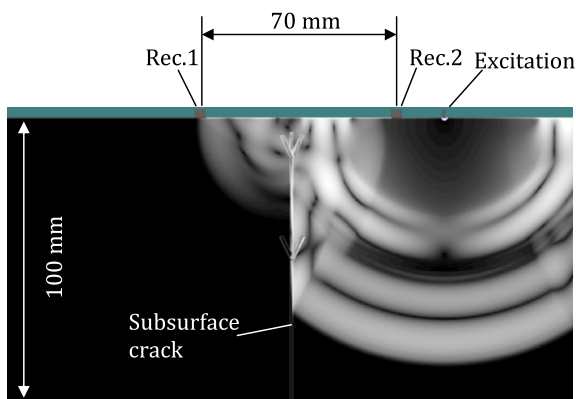


Fig. 14. Geometric model and displacement field after excitation of one cycle of 200 kHz .

shown corresponding to the lowest and highest frequencies tested. These result in Rayleigh wavelengths from 120 mm to 12 mm .

4.3. Experimental results

Testing of specimens with different depths of damage enabled correlation of wave parameters with the thickness of the healthy surface layer between the crack and the surface, apart from simply identification that has been accomplished in an earlier study [11]. Fig. 15a shows the experimental results for velocity of the longitudinal waves for the different depths to crack. The results are normalized to the maximum which is the value on sound material (4222 m/s). It is shown that for material without crack (depth-to-crack considered equal to the specimen thickness of 100 mm) and for crack at the depth of 31 mm the velocity is similar. Therefore, longitudinal wave propagation will give no warning for the underlying crack at this depth. However, as the crack reaches closer to the surface the measured velocity drops and reaches 66% for the specimen with the largest crack (approx. 3 mm from the surface). The results show that in order for damage to be identified by P-wave velocity, which is the most common feature used in

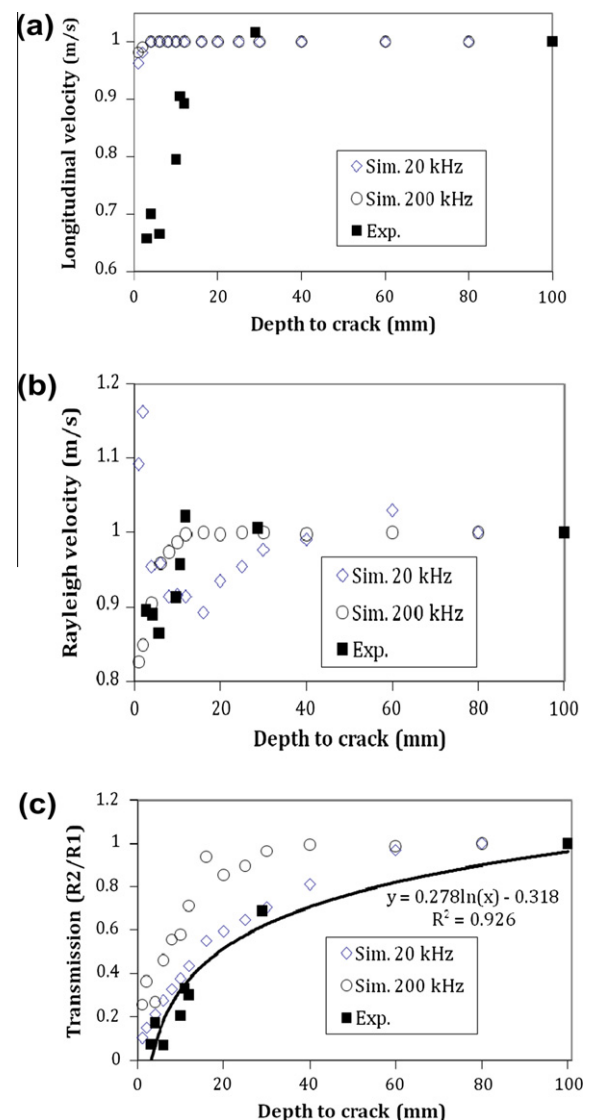


Fig. 15. Wave parameters vs. depth-to-crack: (a) longitudinal velocity, (b) Rayleigh velocity and (c) transmission. The continuous line of Fig. 14c is the fitted curve to the experimental data.

ultrasonics, by one sided measurements, it should be as close as 11 mm in order to result in noticeable decrease (10% for crack 10.6 mm below the surface, see arrow in Fig. 15a).

Fig. 15b shows the corresponding experimental trends for the Rayleigh wave velocity. It also decreases as the crack reaches closer to the surface but the percentage of decrease seems to be lower than longitudinal (less than 15% even for the largest crack). However, it is pointed out that measurement of Rayleigh includes identification of a “typical point” which in most cases is a strong positive or negative peak of the Rayleigh portion [11,19]. In undamaged cases, identification of this point is quite simple, (as seen in Fig. 13b), because the Rayleigh portion of the wave is undistorted. However, for several cases of damaged material in this study, it was difficult to accurately identify the Rayleigh reference point (2nd receiver of Fig. 13c), which certainly reduces the repeatability of this measurement and increases the experimental scatter.

A parameter that can be defined in an absolutely deterministic way is the amplitude of the wave which corresponds to the maximum voltage (V) of the received waveforms, see again Fig. 13b. The difference in amplitudes between the two receivers waveform is reasonable due the geometric spreading of the wave beam [22], as well as damping due to viscous characteristics of the material. In addition to these mechanisms, another very important factor is inhomogeneity which may reflect or scatter the wave to directions other than the original. In the specific case, the subsurface crack blocks the propagation path and therefore, a portion of ultrasonic energy, will not proceed to the second transducer. Therefore, the ratio of the amplitude of the second to the first receiver may well be used as a factor of transmission to correlate with the extent of damage. The results are shown in Fig. 15c. The influence of the crack is much stronger in this feature as it is decreased by more than 10% of the transmission exhibited through sound material. The curve can be fitted by logarithmic increment with quite high correlation coefficient, which shows the smooth influence of damage on this parameter and the nearly monotonic nature of the curve allows estimation of the depth-to-crack. Therefore, from the above experimental analysis it is concluded that the amplitude of the wave is very reliable parameter for correlation with subsurface damage, due to its highest sensitivity as well as the reliability of the measurement which does not use a reference point (sometimes difficult to be identified), and also is not affected by noise, which could mask the initial arrival of the P-wave.

4.4. Numerical results and comparison

Concerning the numerical results, the wave parameters examined, namely P-wave velocity, R-wave velocity and amplitude are depicted as a function of depth-to-crack in Fig. 15a–c. For the case of P-wave (Fig. 15a, there is only a slight decrease (less than 5%) for very shallow cracks, showing that in a homogeneous, non viscous material, the influence of the subsurface crack would not be visible on simple velocity measurements, since this thin layer of healthy material is enough for sufficient wave propagation. The discrepancy between experimental and simulation results highlights the inhomogeneous and damping nature of concrete which is not taken into account in the simulation. Additionally, it is possible that very small cracks extend to the interior of the actual material, without any visual sign from the side. Therefore they influence wave propagation in a more severe way than would be expected by their nominal distance to the surface, as measured from the side. For the Rayleigh wave velocity which is seen in Fig. 15b, a smooth and monotonic trend is resulted only for 200 kHz, with velocity decreasing to 83% of the sound material velocity. For the lowest frequency (20 kHz) the results do not show a clear trend. For very thin sound layers, the velocity increases, which is possibly the effect of mode conversion on top of the crack; it is known that

Rayleigh waves cannot form for slab thicknesses smaller than twice their wavelength [24]. Therefore, for very shallow cracks, the peak identified for velocity measurement may not correspond to pure Rayleigh but may also include other modes after the wave impinged on the crack. Finally, the amplitude ratio (2nd–1st receiver) is depicted in Fig. 15c for both frequencies. It confirms that amplitude is much more sensitive than velocity for damage characterization. For both frequencies, the amplitude ratio drops smoothly with depth-to-crack until 25% of the sound for 200 kHz and 10% for 20 kHz. Results from 20 kHz exhibit constantly lower values, something reasonable since they are influenced even by the cracks deep below the surface, while 200 kHz are clearly influenced only when the crack is 12 mm from the surface, being thus less sensitive to the underlying damage. The simulation results concerning amplitude are in very good accordance with experimental, showing that amplitude is a very reliable parameter to be included in the characterization of subsurface damage. The amplitude value may well be used not only for cracking detection but also for evaluation of the depth, through the monotonic correlation expressed between both experimental and numerical amplitudes (especially for 20 kHz) and depth-to-crack.

4.5. Experimental scatter

In Fig. 15, the points stand for the average of ten measurements as already explained in the text. However, the experimental scatter of the data carry also valuable information. When a material is intact, all possible wave paths are almost identical resulting in similar values of velocity. However, in the presence of cracks, the inhomogeneity is increased and each wave path becomes unique. Therefore, even slight translation or rotation of the sensors array will result in substantial changes in the inspected wave path leading to considerable experimental scatter [11,25]. Fig. 16 shows the coefficient of variation, COV (standard deviation as a percentage of the average) for all different wave parameters. For longitudinal and Rayleigh wave velocity COV is approximately 3% on sound material. This accounts for the inherent inhomogeneity of concrete (bubbles, grains, fibers) as well as possible fluctuations in the sensor coupling conditions. COV increases to 20% for cracks rupturing almost the whole cross section of the specimen. At the same time the COV of amplitude starts at 13% for sound material since amplitude is much more sensitive to inhomogeneity and coupling conditions. For the large cracks though, COV increases up to 45%, exhibiting an exponential dependence on the depth-to-crack, as seen by the fitted line. This shows that apart from the average values, the statistics of the measurement populations can also supply additional descriptors to enhance characterization.

4.6. Frequency

This section aims solely to discuss the behavior of the pulse frequency in order to highlight the additional difficulties posed to the

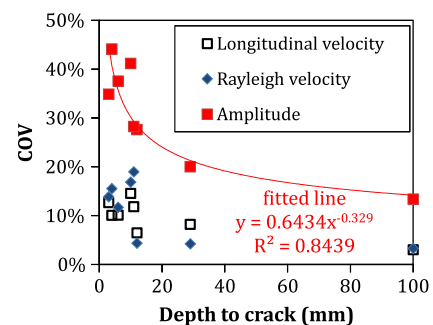


Fig. 16. Coefficient of variation for wave parameter vs. depth-to-crack.

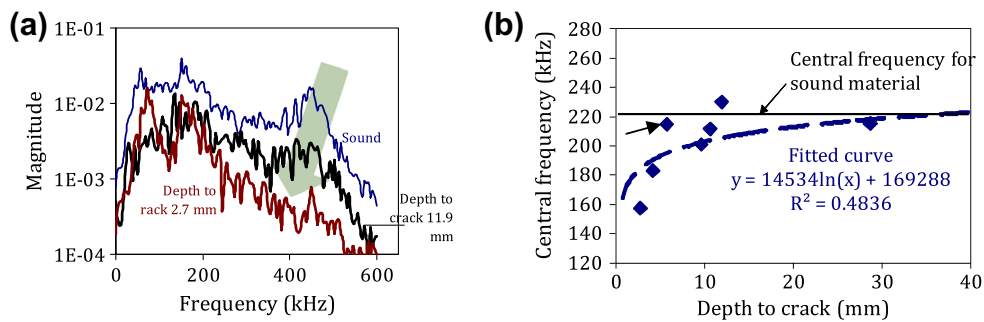


Fig. 17. (a) FFT of the 2nd receiver's response for materials with different subsurface cracks and (b) central frequency vs. depth-to-crack for all specimens.

inspection by the inherently heterogeneous nature of concrete compared to other engineering materials. Frequency has been used for damage estimation based on the fact that scattering attenuation due to inhomogeneity is more effective to higher frequencies and, as a consequence, the frequency content in damaged material is downshifted as the wave propagates [23]. In the present case, the frequency of the pulses was examined using the “central frequency”. It is defined as the centroid of the spectrum after fast Fourier transform (FFT) of the whole length of the time-domain waveform (specifically 2048 points or 204 μ s), similarly to [23]. This was enabled due to the broad band transducers that were used in comparison to resonant ones which have selective response to limited frequency bands. The results show a trend similar to other wave parameters. Fig. 17a shows FFTs of waveforms recorded by the second transducer for the case of intact specimen and specimens with two different depths to crack. The frequency content of around 400 kHz is effectively eliminated for the cracked material, while the lower content does not suffer similar decrease. This has an effect on the central frequency of the envelope, as seen in Fig. 17b. Measurements on sound material result in a central frequency of 222 kHz, while for most cases up to crack 5.7 mm below the surface (see arrow in Fig. 17b), the central frequency falls within 20 kHz from that value. Only for the extreme cases of large cracks there is a substantial frequency drop (158 kHz for the crack of 2.7 mm depth). This result seems contradictory to what would be normally expected for an elastic and homogeneous material; it is reasonable that low frequencies due to their long wavelength and penetration depth should be more effectively blocked, while higher would survive. However, this effect seems to be masked by the inherent attenuation of concrete, owing to damping and scattering on microstructure (air voids and aggregates). This result is also indicative of the difficulties that the heterogeneous nature of concrete, as well as the random geometry of the actual cracking impose on NDT performed by elastic wave propagation.

5. Conclusions

The present study occupies with the development of a methodology to detect and characterize subsurface defects in concrete. The complimentary use of two NDT inspection methods (thermography and ultrasound) shows promising results as to reliability and applicability. According to the above results the methodology would include an initial scanning of the concrete surface by the infrared camera at the time of maximum heat exchange between the structure and environment after direct sunlight. Information from the temperature field (local fluctuations), as well as the cooling down curve (different rate of cooling down relatively to the neighbouring areas) will indicate the subsurface defects. After the “suspicious” areas are selected based on thermography, ultrasonic sensors will be applied on these areas in order to measure the

amplitude and velocity of the propagating wave and correlate to the depth-to-crack.

The basic conclusions are summarized below:

- (1) Simple thermographs at approximately 60 °C reveal the existence of vertical subsurface cracks up to the depth of 11 mm.
- (2) Averaging of the temperature over a mesh direction enhances the estimation by the strong local minima of the curve that correspond to the crack location.
- (3) The cooling down curve from approximately 60–50 °C obtains lower exponential decay coefficient for the areas over the crack compared to areas without crack, even for the small and deep cracks (11 mm from the surface). The above concern cracking (and not only delaminations) which is mainly vertical and therefore has very small projection on the monitored surface.
- (4) Elastic wave propagation parameters are sensitive to the existence of subsurface cracks. The strongest feature for damage characterization is the wave amplitude which is defined easily and changes by more than 95% for cracked material compared to the sound one. The dependence of amplitude on depth-to-crack is monotonic allowing not only damage detection, but also characterization.
- (5) Simulations show good agreement with experimental wave parameters, and confirm that wave amplitude is the most suitable parameter for accurate characterization of depth-to-crack.

The work should continue in the direction of increasing the sensitivity of the methodology for detection of smaller and deeper cracks, as well as check larger specimens, in order to minimize or exclude edge effects.

References

- [1] Thanoon WA, Jaafar MS, Razali M, Kadir A, Noorzaei J. Repair and structural performance of initially cracked reinforced concrete slabs. *Construct Build Mater* 2005;19(8):595–603.
- [2] Ohtsu M, Tomoda Y. Phenomenological model of corrosion process in reinforced concrete identified. *Acoust Emission* 2008;105(2):194–9.
- [3] Clark MR, McCann DM, Forde MC. Application of infrared thermography to the non-destructive testing of concrete and masonry bridges. *NDT&E Int* 2003;36:265–75.
- [4] Weil GJ. Infrared thermographic techniques. In: Malhotra VM, Carino NJ, editors. *Handbook on nondestructive testing of concrete*. Boca Raton: CRC Press; 2004.
- [5] Barreira EV, de Freitas VP. Evaluation of building materials using infrared thermography. *Construct Build Mater* 2007;21:218–24.
- [6] Maierhofer C, Brink A, Rollig M, Wiggenhauser H. Quantitative impulse-thermography as non-destructive testing method in civil engineering – experimental results and numerical simulations. *Construct Build Mater* 2005;19:731–7.
- [7] Naik TR, Malhotra VM, Popovics JS. The ultrasonic pulse velocity method. In: Malhotra VM, Carino NJ, editors. *Handbook on nondestructive testing of concrete*. Boca Raton: CRC Press; 2004.

- [8] Aggelis DG, Momoki S, Chai HK. Surface wave dispersion in large concrete structures. *NDT & E Int* 2009;42:304–7.
- [9] Selleck SF, Landis EN, Peterson ML, Shah SP, Achenbach JD. Ultrasonic investigation of concrete with distributed damage. *ACI Mater J* 1998;95(1):27–36.
- [10] Shiotani T, Momoki S, Chai H, Aggelis DG. Elastic wave validation of large concrete structures repaired by means of cement grouting. *Construct Build Mater* 2009;23(7):2647–52.
- [11] Aggelis DG, Kordatos EZ, Soulioti DV, Matikas TE. Combined use of thermography and ultrasound for the characterization of subsurface cracks in concrete. *Construct Build Mater* 2010;24:1888–97.
- [12] Cheng CC, Cheng TM, Chiang CH. Defect detection of concrete structures using both infrared thermography and elastic waves. *Automation in Construction* 2008;18:87–92.
- [13] Soulioti DV, Barkoula NM, Paipetis A, Matikas TE. Effects of Fibre Geometry and Volume Fraction on the Flexural Behaviour of Steel–Fibre Reinforced Concrete. *Strain*, in press, doi: 10.1111/j.1475-1305.2009.00652.x.
- [14] Maldague X. *Theory and practice of infrared technology for non destructive testing*. New York: John-Wiley & Sons; 2001.
- [15] Sham FC, Chen N, Long L. Surface crack detection by flash thermography on concrete surface. *Insight* 2008;50(5):240–3.
- [16] Sakagami T, Kubo S. Development of a new non-destructive testing technique for quantitative evaluations of delamination defects in concrete structures based on phase delay measurement using lock-in thermography. *Infrared Phys Technol* 2002;43:311–6.
- [17] Matsuyama K, Yamada M, Ohtsu M. On-site measurement of delamination and surface crack in concrete structure by visualized NDT. *Construct Build Mater* 2010;24:2381–7.
- [18] Aggelis DG, Shiotani T, Polyzos D. Characterization of surface crack depth and repair evaluation using Rayleigh waves. *Cem Concr Compos* 2009;31(1):77–83.
- [19] Qixian L, Bungey JH. Using compression wave ultrasonic transducers to measure the velocity of surface waves and hence determine dynamic modulus of elasticity for concrete. *Construct Build Mater* 1996;4(10):237–42.
- [20] Wave2000, Cyber-Logic, Inc., NY (<<http://www.cyberlogic.org>>).
- [21] Kaufman JJ, Luo G, Siffert RS. Ultrasound simulation in bone. *IEEE Trans Ultrason Ferroelectri Freq Contr* 2008;55(6):1205–18.
- [22] Owino JO, Jacobs LJ. Attenuation measurements in cement-based materials using laser ultrasonics. *J Eng Mech. ASCE* 1999;125(6):637–47.
- [23] Shiotani T, Aggelis DG. Wave propagation in concrete containing artificial distributed damage. *Mater Struct* 2009;42(3):377–84.
- [24] Zerwer A, Polak MA, Santamarina JC. Rayleigh wave propagation for the detection of near surface discontinuities: finite element modeling. *J Nondestruct Eval* 2003;22(2):39–52.
- [25] Aggelis DG, Shiotani T. Experimental study of surface wave propagation in strongly heterogeneous media. *J Acoust Soc A* 2007;122(5):EL151–157.